Applied Microscopy
Korean Society of Microscopy

pISSN 2287-5123 · eISSN 2287-4445
https://doi.org/10.9729/AM.2017.47.3.131

Regular Article

Electric Conduction Mechanisms Study within Zr Doped Mn_3O_4 Hausmannite Thin Films through an Oxidation Process in Air

L. Ben Said[1,2,*], R. Boughalmi[1], A. Inoubli[3], M. Amlouk[1,2]

[1]*Unit of Physics of Semiconductor Devices, Faculty of Science of Tunis, Tunis El Manar University, Tunis 2092, Tunisia*
[2]*Faculty of Science of Bizerte, Carthage University, Zarzouna 7021, Tunisia*
[3]*Laboratory of Physics of Lamellar and Nanomaterial Materials, Hybrids (LPMLNMH), Faculty of Science of Bizerte, Carthage University, Zarzouna 7021, Tunisia*

*Correspondence to:
Said LB,
Tel: +216-58-147-883
E-mail: bensaidlilia@gmail.com

Received September 8, 2017
Revised September 12, 2017
Accepted September 12, 2017

In this work further optical and electrical investigations of pure and Zr doped Mn_3O_4 (from 0 up to 20 at.%) thin films as a function of frequency. First, the refractive index, the extinction coefficient and the dielectric constants in terms of Zr content are reached from transmittance and reflectance data. The dispersion of the refractive index is discussed by means of Cauchy model and Wemple and DiDomenico single oscillator models. By exploiting these results, it was possible to estimate the plasma pulse ω_p, the relaxation time τ and the dielectric constant ε_∞. Second, we have performed original ac and dc conductivity studies inspired from Jonscher model and Arrhenius law. These studies helped establishing significant correlation between temperature, activation energy and Zr content. From the spectroscopy impedance analysis, we investigated the frequency relaxation phenomenon and hopping mechanisms of such thin films. Moreover, a special emphasis has been putted on the effect of the oxidation in air of hausmannite thin films to form Mn_2O_3 ones at 350°C. This intrigue phenomenon which occurred at such temperature is discussed along with this electrical study. Finally, all results have been discussed in terms of the thermal activation energies which were determined with two methods for both undoped and Zr doped Mn_3O_4 thin films in two temperature ranges.

Key Words: Mn_3O_4, Zr doping, Thin films, Impedance spectroscopy, Oxidation

INTRODUCTION

The electrical conductivity spectroscopy is a powerful technique for the investigation of the ion transport processes. Currently, the frequency dependence of the conductivity can be controlled in a frequency range from mHz up to infrared frequencies. No other experimental method provides a comparable dynamics resolution. In transition metal oxides and their mixed systems, the electrical conduction has been studied extensively due to its incompletely filled 3d shell (Alonso-Domínguez et al., 2016; Baghizadeh et al., 2015; Biju & Khadar, 2003; Boukhachem et al., 2016; Dridi et al., 2015; Khumpaitool & Khemprasit, 2014; Rouahi et al., 2016; Wypych et al., 2014). Among these metal oxides family, hausmannite Mn_3O_4 has attracted much interest due to its typical intrinsic p-type conductivity (Bose & Biju, 2015a, 2015b; Larbi et al., 2014; Ulutas et al., 2016). It is worth noting that in Mn_3O_4, Mn exhibits different oxidation states including divalent Mn^{2+} and trivalent Mn^{3+} ions located at the tetrahedral and octahedral sites, respectively, which makes it one of the most stable manganese oxide. In addition to its stability, the study of the electrical transport phenomena in Mn_3O_4 seems so far in demand for various applications such as: lithium-ion batteries (Zhen et al., 2016), supercapacitors

(Luo et al., 2016; Xu et al., 2015; Yadav et al., 2016), catalysts and sensors (Saputra et al., 2013; Sharma et al., 2016) because of its low-cost, high natural abundance, great environmental compatibility and good specific capacity. Hausmannite Mn_3O_4 thin films have been deposited by several techniques such as: the vapor phase growth method (Chang et al., 2005), the pulse laser deposition (Liu et al., 2014), the polyol process (Jin et al., 2015), the epitaxy (Huang et al., 2015), the hydrothermal method (Dong et al., 2013), the chemical bath deposition (Xu et al., 2006), the chemical successive ionic layer adsorption and reaction (SILAR) process (Gund et al., 2013) and the spray pyrolysis technique (Larbi et al., 2014). Among these deposition methods, the spray pyrolysis with safe, as cost-effective method is widely used to prepare thin film oxides with large surface area for several technological applications. In the present work, this technique is selected to prepare Mn_3O_4 thin films. In this binary oxide, contrary to classical semiconductors, the conduction is caused by a jumping of charge carriers from the low valance state Mn^{2+} to the high valance one Mn^{3+} (Lee et al., 1993). In spite that Mn_3O_4 has also been revealed to be no toxic, its intrinsic insulating properties (Wei et al., 2011) limited the practical applications of such oxide. So, to improve the electronic conductivity and in order to enhance the capacitance of Mn_3O_4 material, a promising approach is to dope it to settle conductivity and band gap of this oxide for the potential applications mentioned above. As previously reported, the doping effect has been widely studied by means of the substitution of Mn in Mn_3O_4 by several transition metal ions like Zn, Sn, Cu, Cr and Ni. In fact, Jha et al. (2012) found that the substitution of Zn seems beneficial to increase the band gap energy of Mn_3O_4 nanorods. Also, Zhao et al. (2014) reported that Sn doped Mn_3O_4/C nanocomposites can be considered as a supercapacitor electrode with higher capacitance. Moreover, it was already shown that spinel-type Cu doped Mn_3O_4 microcrystal can be an effective reagent for the degradation of organic contaminants in water (Larbi et al., 2015b). Lately, in our group, Larbi et al. (2015b) also investigated the micro-structural evolution, the opthothermal and the electrical properties of Mn_3O_4 thin films and they found that the band gap energy can be adjusted from 2.2 to 1.9 eV with Ni content. In addition, Hall measurements showed that Mn_3O_4 thin films exhibit p-type conductivity and this character is reinforced with increasing Ni concentration (Zhi et al., 2000). To date, in previous reports, the doping with Zr as transition-metal ion seems to be beneficial to perform various materials physical properties including optical, electrical and dielectric properties. For instance, many attempts reported already on the effect of Zr doping on $BaTiO_3$ perovskite material. Zhi et al. (2000) found that a compositional variation of Zr in the range of $0.03<x<0.08$ exhibits excellent piezoelectric properties, and with higher Zr concentration (x up to 0.4) a typical relaxor behavior is observed. On the other hand, Tang et al. (2004) reported that Zr content in $BaTiO_3$ affects the transition temperature T_m by shifting it to a lower temperature domain with increasing Zr content which is an interesting result in many applications such as tunable capacitor ones. Moreover, Sun et al. (2014) observed that the dielectric constant as a function of temperature showed a decrease in Curie temperature (T_C) with increasing Zr concentration. Similarly, Aghayan et al. (2014) reported that a significant increase in the permittivity of Zr doped $BaTiO_3$ material was revealed as well as the best dielectric properties and a ferroelectric behavior were found for Zr content equal to x=0.05. Furthermore, zirconium doping in ZnO matrice has been used extensively. Indeed, Hou et al. (2016) noted that suitable the electronic conductivity has been obtained for this oxide using this type of doping. Also, some theoretical studies have been made to investigate the effect of Zr in ZnO matrices. For instance, Wang et al. (2008) examined the structural, optical and electrical properties of zirconium-doped zinc oxide and found that the electronic structure calculations display that when Zr substitute Zn into ZnO, the Fermi-level shifts to the conduction band, and there are excess electrons in this band, which may be a possible enhancement of the electrical conductivity in Zr doped ZnO film (Wang et al., 2008). In the same context, an ab initio study showed that the calculated electrical conductivities of Zr doped ZnO exhibit desirable values which makes this doped oxide attractive for transparent conducting oxide applications (Slassi et al., 2015). On the other hand, other materials were doped with Zr element especially NiO binary oxide which achieved high dielectric constant and low dielectric loss (Mohamed et al., 2016). In the same line, Zr doped $MgTiO_3$ thin films exhibited also high dielectric constant and low loss tangent (Gogoi et al., 2015). Moreover, Zr doped In_2O_3 thin films showed low resistivity (6.4×10^{-4} Ω cm) and higher carrier concentration (2.5×10^{20}) at a doping ratio of 7 at.% (Manoharan et al., 2015) and at last but not at least Zr doped TiO_2 sprayed thin films pointed out an increase by more times of the dielectric constant with Zr doping (Juma et al., 2016). The list of various metal oxide materials that have been doped with zirconium is even longer and more informative (Bai et al., 2016; Lin et al., 2015; Myung et al., 2015; Nicon et al., 2016; Pang et al., 2016; Saini et al., 2016; Shanmugam et al., 2014; Sun et al., 2015; Thongbai et al., 2014; Wei et al., 2015; Zhang et al., 2008). However, for the best of our knowledge, until today there is neither deeply optical dispersion investigation nor electrical study on sprayed Zr doped Mn_3O_4 thin films. With this motivation, the doping of Mn_3O_4 by tetravalent Zr transition metal is explored in this work and the main objective of such study is to explore the optical dispersion of Mn_3O_4 thin films as well as their electrical properties by means of both reflectance-transmittance. In the

same way, ac conductivity measurements have been carried out in the frequency range extended from 5 Hz to 13 MHz therefore covering the behavior from practically dc conduction to high frequency regime where usually electronic processes dominate over ionic conduction process. Herein, for the first time and by means of the electrical conductivity measurements as a function of the temperature, we investigate under the framework of phase transition phenomenon which can occur during air oxidation of hausmannite sprayed thin films which meets the change of concentration of Mn^{2+} ions in those of Mn^{3+} ones within Mn_3O_4 matrix to give Mn_2O_3 phase. The latest regarding the phase transition is considered as the main goal of the present contribution.

MATERIALS AND METHODS

Films Preparation

Zirconium doped manganese oxide thin films (Mn_3O_4:Zr) were deposited onto the glass substrates by the spray pyrolysis technique at 350°C using 0.1 M Manganese chloride ($MnCl_2$_$6H_2O$) solution dissolved in 100 mL of deionized water. To this starting solution, we added ($ZrCl_4$_$6H_2O$) as doping agent at various [Zr]/[Mn] molar ratios: 3, 6, 12, and 20 at.%. The resulting solution was sprayed at a rate flow of 4 mL/min using nitrogen gas. The distance between nozzle and substrate was about 27 cm. After the deposition, the samples were allowed to cool slowly to room temperature.

Characterization Technique

The electrical properties of real and imaginary components of impedance parameters (Z' and Z") were obtained using a Hewlett–Packard 4192 analyzer over a wide range of temperature (320°C~450°C) and frequency (5 Hz~13 MHz). Metallic electrodes were painted on the two extremities of the sample using silver paste. The ac conductivity is calculated using the relation: σ_{ac}=d/Z'A, where Z', d and A are respectively real part of impedance, distance between electrodes and cross-sectional area as displayed in Fig. 1.

RESULTS AND DISCUSSION

Optical Dispersion of Undoped and Zr Doped Mn_3O_4

Optical constants by optical dispersion models

The study of the dispersion of incident photon energy plays an important role in the investigation of the optical properties of a material. Fig. 2 shows the refractive index n (λ) and the extinction coefficient k (λ) spectra of undoped and Zr doped Mn_3O_4 thin films. The extinction coefficient k spectrum shows an obvious decrease versus wavelength and reaches the lowest values in the visible and near infrared ranges which attests the transparency property of Mn_3O_4 thin films. In the wavelength ranging from 300 nm to 700 nm, the refractive index is found to decrease with the wavelength which represents a normal dispersion. Two approaches could be taken to model this behavior. The first is based on the

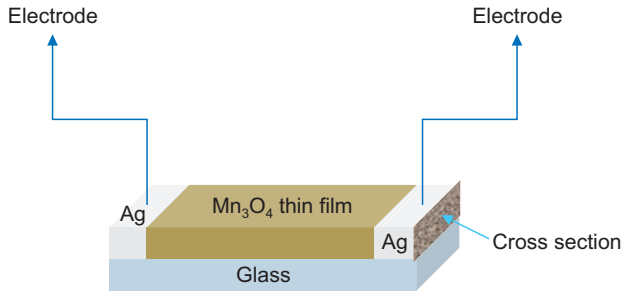

Fig. 1. Configuration of substrate/Mn_3O_4 thin film/Ag samples for the electrical measurements.

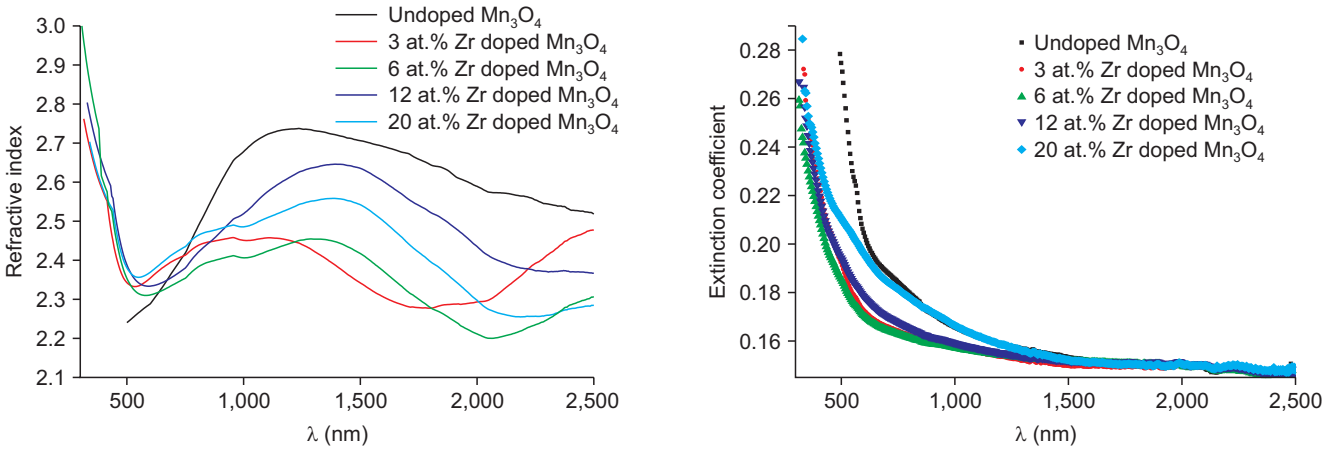

Fig. 2. Refractive index n (λ) and extinction coefficient k (λ) of undoped and Zr doped Mn_3O_4 thin films.

Cauchy dispersion model and the second used Wemple and DiDomenico single-oscillator one. These two models will be detailed below. However, it is observed that the refractive index increases in 700~1,300 nm domain indicating the existence of an absorption zone where the dispersion is abnormal corresponding well to the gap energy. It is also found that in this zone the dispersion decreases significantly after doping, especially for 3 at.% Zr doped Mn_3O_4 film. This may be due to the formation of segregated ZrO_2 which inhibits the displacement of free carriers. Over the wavelength range λ>1,300 nm, the dispersion becomes normal again which may be due to the inertia of the asperities related to ZrO_x oxides. Following zirconium doping, the appearance of another absorption zone above 2,000 nm for both 3 at.% and 6 at.% Zr doped Mn_3O_4 samples is also depicted which could be attributed to the appearance of a new Zr level in the band gap energy. This decrease regarding the refractive index n and the extinction coefficient k values after doping are detected suggesting an optical windows application of the Zr doped Mn_3O_4 thin films as previously shown via photoluminescence study (Said et al., 2017). Outside these absorption zones, since the films are optically transparent in the visible range and for photons energies below the band gap energy ($E<E_g$), the refractive index n (λ) could be modeled according to Cauchy dispersion expression:

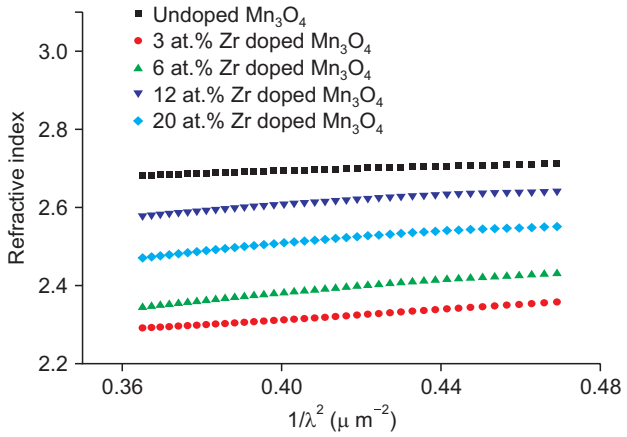

Fig. 3. Refractive index vs. $1/\lambda^2$, in the visible range, of undoped and Zr doped Mn_3O_4 thin films.

Table 1. Values of A and B constants relative to the Cauchy model for each doping level along with other relevant constants

Zr concentration (at.%)	A	B (μm^2)	E_0 (eV)	E_d (eV)
0	2.579	0.285	14.78	2.60
3	2.049	0.656	5.84	1.71
6	2.033	0.863	5.37	1.55
12	2.297	0.777	7.47	1.67
20	2.25	0.956	5.62	1.48

$$n(\lambda) = A + \frac{B}{\lambda^2} \quad (1)$$

where A and B are Cauchy parameters and the unit of wavelength is μm. The variations of n as a function of λ^2 are displayed in Fig. 3. The final values of A and B were determined by fitting the model-generated data to the experimental ones and are gathered in Table 1. In the same zone (i.e., in the visible spectral range as shown in the inset of Fig. 2), in addition to the Cauchy model, the curves n (λ) below the inter-band absorption edge shows a Sellmeier dispersion type dependence as reported in literature (Mardare & Hones, 1999) and could be thus studied by means of the Wemple and DiDomenico single-oscillator model to investigate the average excitation energy E_0 and dispersion energy E_d of the deposited material (DiDomenico et al., 1969; Wemple & DiDomenico, 1971). According to this model, the refractive index is related to the energy of the incident photons by the following expression:

$$\frac{1}{n^2-1} = \frac{E_0^2 - (h\nu)^2}{E_0 E_d} \quad (2)$$

where E_0 and E_d are the single-oscillator energy and dispersion energy parameter, respectively. By using relation (2) in the following form:

$$\frac{1}{n^2-1} = \frac{E_0}{E_d} - \frac{(h\nu)^2}{E_0 E_d} \quad (3)$$

We can plotted $(n^2-1)^{-1}$ vs. $(h\nu)^2$ for different doping levels and the values of E_0 and E_d are directly determined from the slope of $(E_0E_d)^{-1}$ curves and the intercept of (E_0/E_d) on the vertical axis, Fig. 4. These values are gathered in Table 1. In the literature, the dispersion parameters of several materials were investigated based on this model (Caglara et al., 2007; Mrabet et al., 2015; Ouni et al., 2010; Park, 2012). As expected, E_d

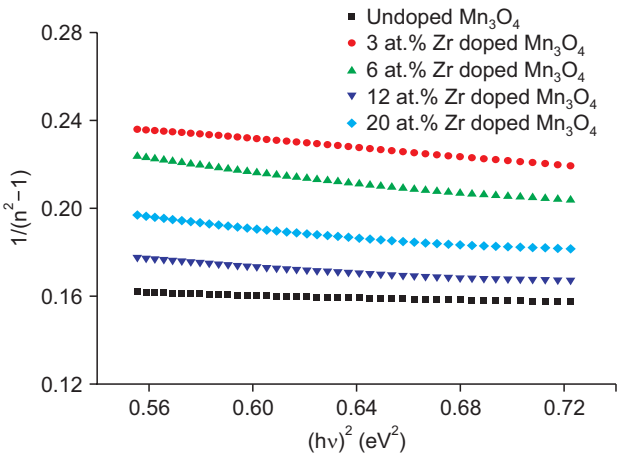

Fig. 4. Plots of as a function of $(h\upsilon)^2$, in the visible range, for different doping level.

value decreases with Zr content leading to an increase of the optical dispersion phenomenon.

Optical dielectric characterization and optical conductivity

The complex dielectric constant ε (λ) characterizes the optical properties of a solid material. Using n and k calculated data, the dielectric constants are deduced from the following system:

$$\begin{cases} \varepsilon_1(\lambda) = n^2(\lambda) - k^2(\lambda) \\ \varepsilon_2(\lambda) = 2n(\lambda)\ k(\lambda) \end{cases} \quad (4)$$

The variations of $\varepsilon_1(\lambda)$ and $\varepsilon_2(\lambda)$ are given in Fig. 5. In the near infrared region, when n^2 is higher than k^2, and $\omega\tau<<1$, the real and imaginary parts of the dielectric constant can be expressed by the following relations (Belgacem & Bennaceur, 1990):

$$\varepsilon_1 = \varepsilon_\infty - \frac{\varepsilon_\infty \omega_p^2}{4\pi^2 c^2}\lambda^2$$
$$\varepsilon_2 = \frac{\varepsilon_\infty \omega_p^2}{(2\pi c)^3 \tau}\lambda^3 \quad (5)$$

where τ is the relaxation time, ε_∞ is the high frequency limit of the dielectric constant and ω_p is the plasma frequency given by:

$$\omega_p^2 = \frac{4\pi\ Ne^2}{\varepsilon_\infty m_e^*} \quad (6)$$

with N being the charge carrier's density and m_e^* is the effective mass of the charge carrier.

The variations of $\varepsilon_1(\lambda)$ as a function of λ^2 and $\varepsilon_2(\lambda)$ as a function of λ^3 are represented in Fig. 6. It is found that, in the infrared range, ε_1 is a linear function with λ^2 while ε_2 is linear with λ^3, allowing thus to determine ε_∞, ω_p, τ and $\frac{Ne}{m_e^*}$. Their calculated values are summarized in Table 2. The value of ε_∞ of about 8 is higher than those of La doped NiO and Li doped ZnO binary ones. However, ω_p values remain in $3\sim9\times10^{14}$ rd/s domain which matched well with those of the same oxides (Mrabet et al., 2016; Salah et al., 2017).

Electrical Conductivity Study

The impedance spectroscopy is considered as a powerful

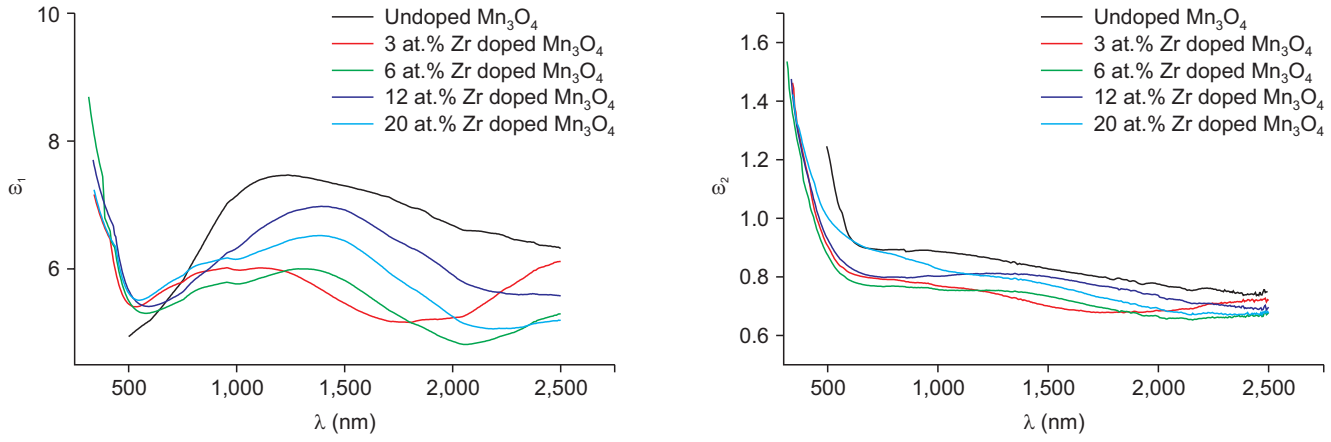

Fig. 5. Dielectric constants ε_1 (λ) and ε_2 (λ) of undoped and Zr doped Mn_3O_4 thin films.

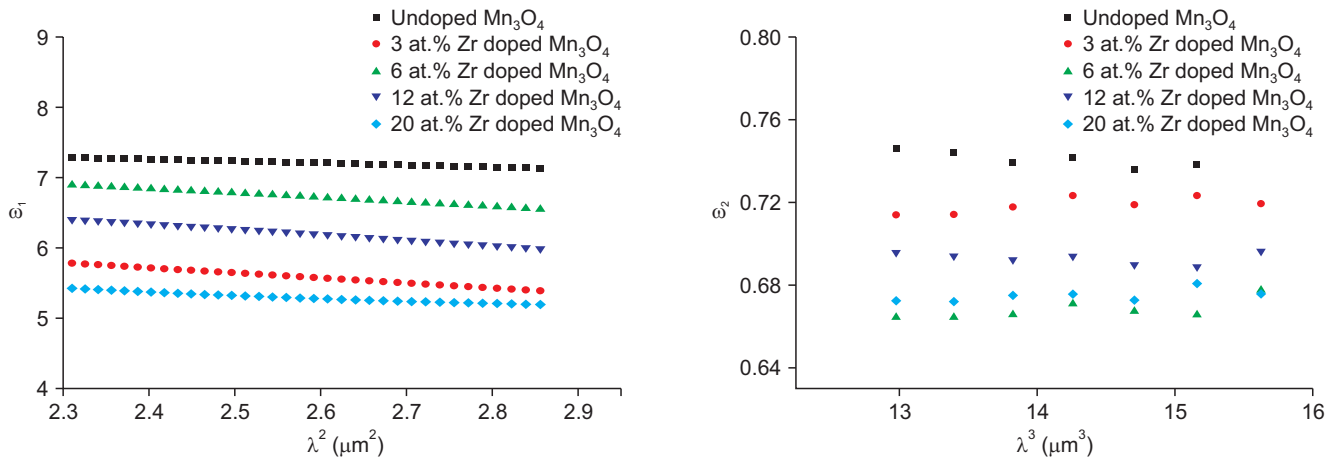

Fig. 6. ε_1 vs. λ^2 and ε_2 vs. λ^3 of undoped and Zr doped Mn_3O_4 thin films.

Table 2. Values of the dielectric parameters deduced from optical measurements

Zr concentration (at.%)	ε_∞	ω_p (10^{14} rad s^{-1})	T (10^{-14} s)	N/ m_e^* (10^{48} cm^{-3} g^{-1})
0	7.94	3.54	2.62	3.43
3	6.38	4.64	2.14	4.73
6	7.46	5.85	3.24	8.80
12	8.36	7.9	3.34	18.00
20	8.19	5.78	5.02	9.43

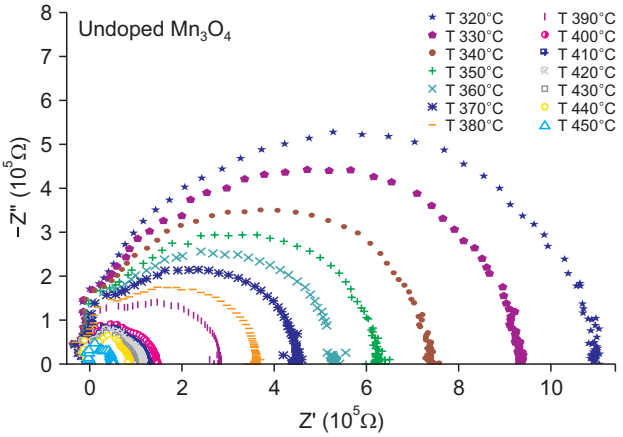

Fig. 7. Complex impedance spectra as a function of temperature of undoped Mn_3O_4 thin film.

technique to investigate the performance of the electrical conduction mechanisms inside a thin film material. In this work, the impedance data plots are used to determine both dc and ac conductivity of Mn_3O_4:Zr thin films.

Undoped Mn_3O_4 thin films

The impedance analysis

Nyquist plots (–Z" vs. Z') of undoped Mn_3O_4 thin film extracted from the impedance spectroscopy measurements in the temperature range from 320°C to 450°C with a pitch of 10°C are given in Fig. 7. Generally, the impedance analysis provides the information about the contribution of the relaxation process of different micro regions in the polycrystalline material such as grain, grain boundary and electrode interfaces, the semi-circle behavior of complex impedance plots of each micro region could be thus explained on the basis of an equivalent circuit model consisting of a combination series of grain (high frequency region) and grain boundary elements boundaries (low frequency region) (Larbi et al., 2014; Luo et al., 2016; Xu et al., 2015; Yadav et al., 2016; Yang et al., 2016). So, characteristically, two semi-circular arcs should be observed with non-zero high-frequency intercepts. However, as can be seen in the diagrams, the display of impedance data in the complex plane plot appears

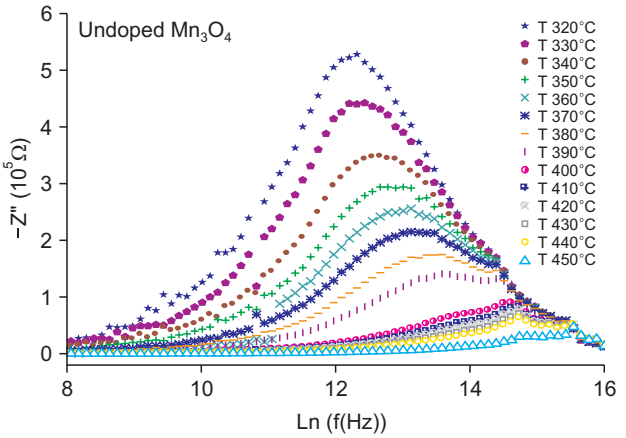

Fig. 8. Frequency dependence of Z'' at various temperatures of undoped Mn_3O_4 thin film.

in the form of succession of only one depressed semicircle (in each temperature) indicating a non-Debye relaxation of the electrical ac response. This remains with the absence of a second semicircle confirming that the polarization mechanism corresponds to the bulk effect arising in a semi conductive grain. From the features of these semicircles, it can be deduced that the resistance of the thin films decreases with the temperature indicating a semiconducting behavior of hausmannite thin film manifested by the thermal activation of the electrical conduction in both ac and dc regimes. The variations of the imaginary part Z" of the complex impedance of undoped Mn_3O_4 as a function of the frequency, for different temperatures, are represented in Fig. 8. As could be seen, for a given temperature, Z" increases with frequency and a relaxation peak is developed in the spectra, which is shifted to the high frequency side with increasing the temperature showing a decrease in amplitude. This implies that the transient polarization phenomenon is temperature dependent and could be explained as follows: at high temperature, the steady state conduction mechanism is attained rapidly instead of a long time as at low temperatures. However, at high electric fields, whatever the temperature, the steady state is reached almost instantly suggesting that these polarization effects predominate only at low fields. The maximum of Z" gives the relaxation frequency f_{Max} which is governed by Arrhenius law:

$$f_{Max} = f_0 \exp\left(-\frac{E_A}{kT}\right) \quad (7)$$

where E_A is the activation energy of the relaxation process and f_0 is a characteristic frequency expressed by $2\pi f_0\tau=1$ where τ corresponds to the characteristic relaxation time of the phonons. From Fig. 9 two temperature ranges could be distinguished; for high temperatures (>420°C) the activation energy is of the order of E_{A2}=0.24 eV which is lower compared

to that determined for the lowest temperatures (E_{A1}=0.70 eV) confirming thus an important dependence of the electrical conduction with the temperature (Table 3).

Conductivity study

ac conductivity. Fig. 10 reveals the frequency dependent conductivity of undoped Mn_3O_4 thin film at different temperature ranges. It can be seen that the frequency dependence of conductivity shows two distinct regimes: i) at lower frequencies and at higher temperatures, the conductivity shows a flat response (the presence of plateau) corresponding to the frequency independent conductivity σ_{dc} obtained by extrapolating the conductivity value to the lower frequency. This could be attributed to the long range transport of the mobile ions in response to the electric field, where the only successful jumps to its neighborhood vacant site due to the available long time period contributes to the yields dc conductivity σ_{dc} as explained previously by Funke using a jump relaxation model (Funke, 1993; Mahajan et al., 2014). ii) In the high frequency region (dispersion region), the conductivity has an ω^s dependence and can be explained in terms of polaron hopping, using Jonscher's power law:

$$\sigma = \sigma_{dc}(1 + A\omega^s) \quad (8)$$

where σ is the ac conductivity, σ_{dc} is the limit of a zero

Table 3. Some electrical parameters of the Zr doped Mn_3O_4.

Zr concentration (at.%)	Activation Energy (eV)				W_m (eV)
	$E_{A(Z^{''})}$		$E_{A(\sigma_{DC})}$		
	$E_{A_1(Z^{''})}$	$E_{A_2(Z^{''})}$	$E_{A_1(\sigma_{DC})}$	$E_{A_2(\sigma_{DC})}$	
0	0.70±0.02	0.24±0.05	0.69±0.03	0.57±0.01	1.5±0.2
3	0.54±0.03	0.38±0.04	0.63±0.02	0.72±0.05	1.83
6	1.06±0.04		0.9 ±0.02		2.30
12	0.48±0.03	1.15±0.07	0.72±0.04	0.38±0.03	2.40±0.3
20	0.87±0.04	0.16±0.02	0.78±0.03	0.83±0.14	-

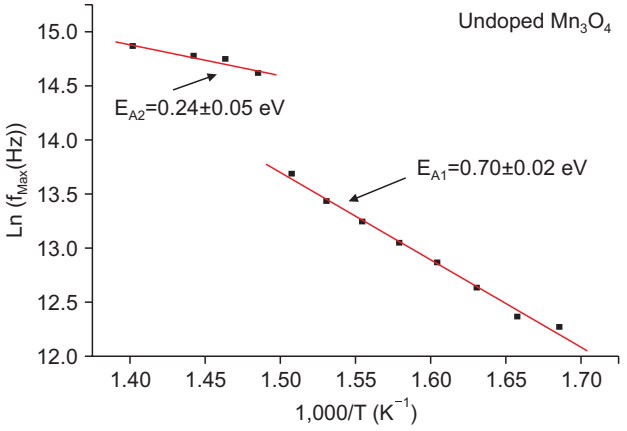

Fig. 9. Plot of ln(f_{Max}) versus 1,000/T of undoped Mn_3O_4 thin film.

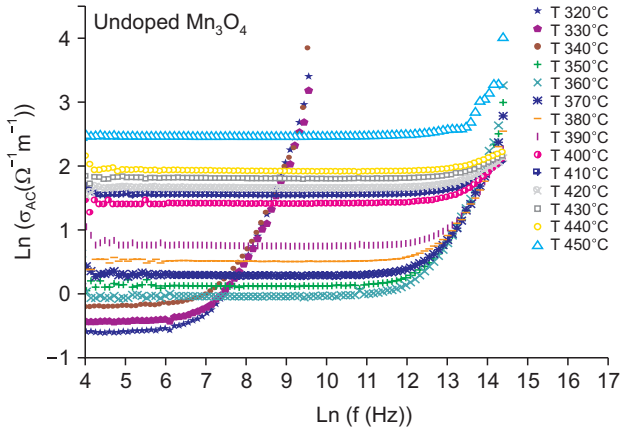

Fig. 10. Plot of ac conductivity as a function of frequency at different temperatures for undoped Mn_3O_4 sample.

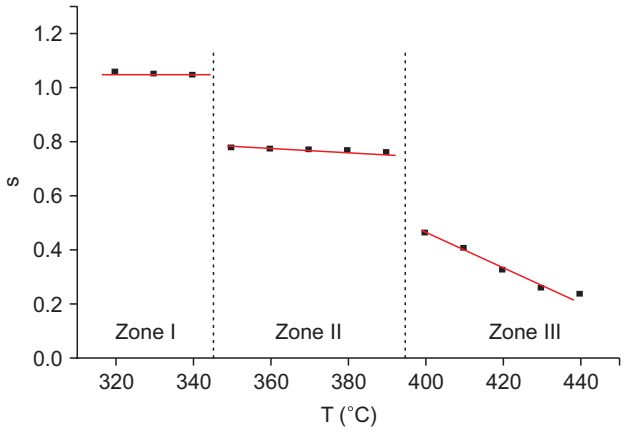

Fig. 11. Temperature dependence of the angular frequency exponents.

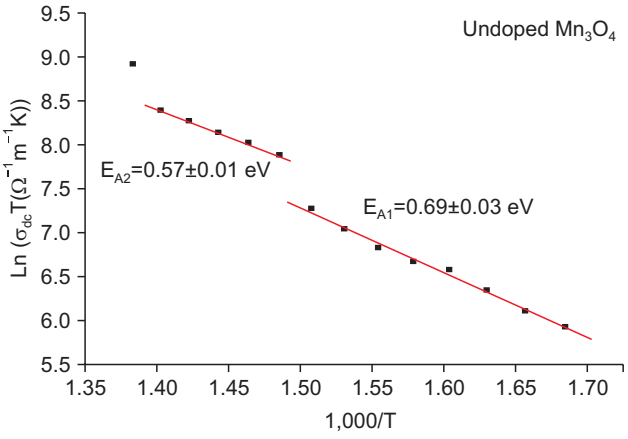

Fig. 12. Plot of Ln (σ_{dc}T) versus 1,000/T.

frequency conductivity, A is a pre-exponential constant, $\omega=2\pi f$ is the angular frequency and "s" is the material intrinsic property dependent constant. From the same figure (Fig. 10), it is observed that the high frequency dispersion region starts to decrease and disappears by increasing the temperature. Thereby, the characteristic frequency ω_p also known as the hopping frequency, at which the relaxation effects begin to appear, moves towards the higher frequency with the increase of the temperature. As shown in Fig. 11, the electrical conduction mechanism is tributary to "s" values. In fact, three

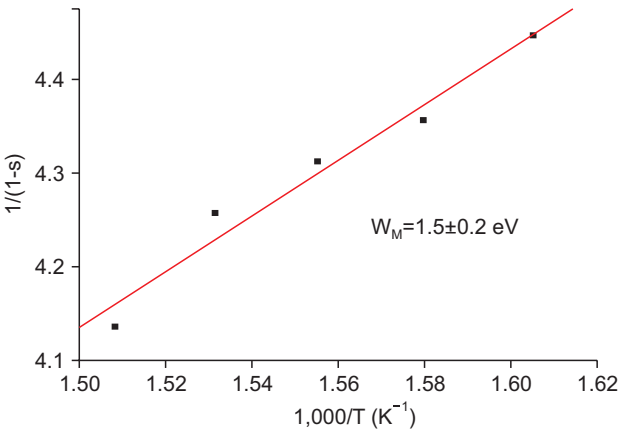

Fig. 13. Plot of W_M for pure Mn_3O_4 film.

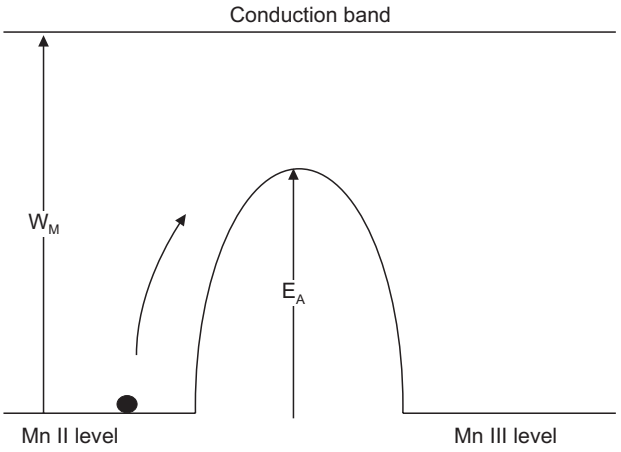

Fig. 14. Energetic diagram of defects in Mn_3O_4 sprayed thin film.

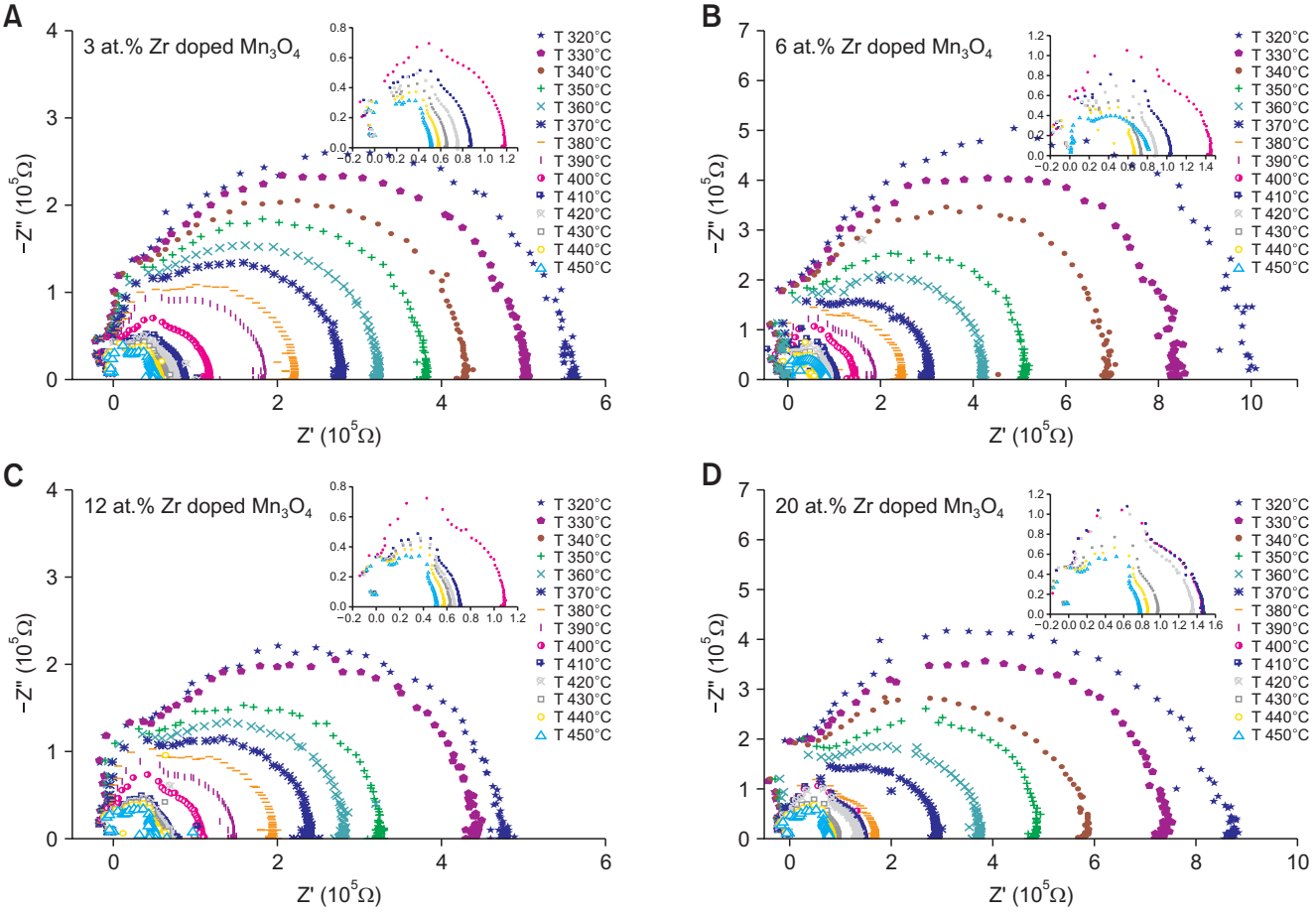

Fig. 15. Complex impedance spectra as a function of temperature of 3 at.% (A), 6 at.% (B), 12 at.% (C), and 20 at.% (D) Zr doped Mn_3O_4 films.

different regions could be distinguished:

- A low-temperature region (<350°C), for which the activation is performed at low frequency (~2 KHz) with high and constant exposure (same slope).
- A region of intermediate temperatures (350°C~390°C) in which the conduction is activated at high frequencies (~40 KHz) with a power exponent of the order of "s=1" that decreases with the temperature suggesting that the correlated barrier hopping (CBH) model may be suitable to explain the conduction mechanism in Mn_3O_4 thin film.
- A region of relatively high temperatures (≥400°C) in which the conduction is activated at high frequencies (~40 KHz) with "s" value lower than 0.5 showing a decrease with the temperature.

Different hopping mechanisms are reported to predict temperature dependent value of "s". A more detailed explanation will be presented in detail in the following sections.

σ_{dc} behavior. The variation of σ_{dc} with temperature is shown in Fig. 10. As it could be seen, the dc conductivity increases with the temperature proving that the conduction is thermally activated, and may obey to Arrhenius law:

$$\sigma_{dc} = \frac{A}{T}\exp\left(-\frac{E_A}{kT}\right). \quad (9)$$

To reach the activation energy values, $\mathrm{Ln}(\sigma_{dc}T)$ curves are plotted in terms of the inverse of the temperature, Fig. 12. Two activating energies were observed. At low temperature, the conductivity shows an activation energy of approximately 0.69 eV, matching well with that found along the frequency study, which implies that the static (long range of nature) and dynamic behaviors are of the same scope. However, at high temperatures, the activation energy is found to be equal to 0.57 eV significantly greater than that of the frequency study, proving that the two relaxation processes are of different scope. Generally, at low frequencies, the dominant polarization process in undoped Mn_3O_4 thin film may be explained as a local displacement of electrons by hopping mechanism between Mn^{2+} and Mn^{3+} ions and an orientation

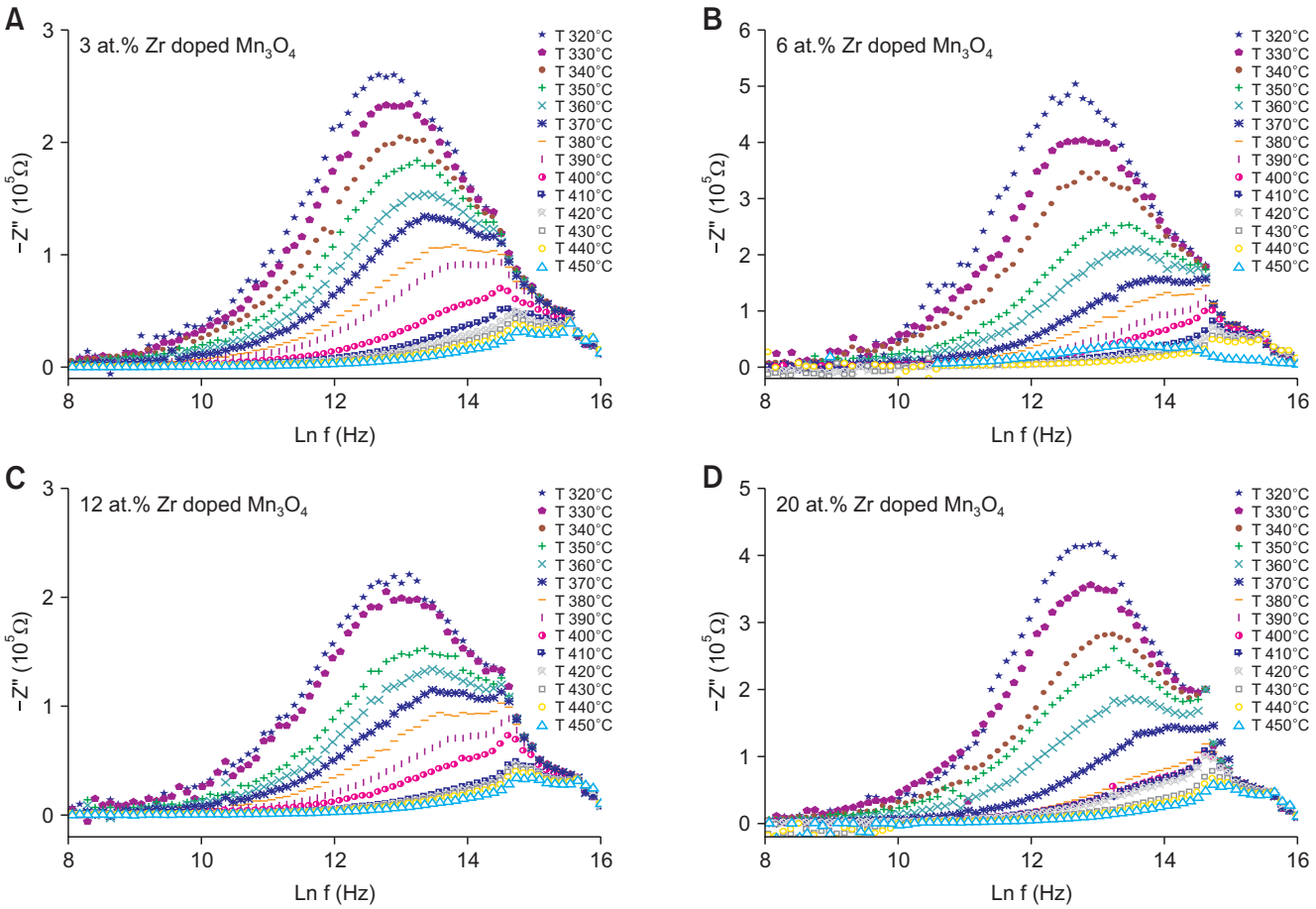

Fig. 16. Frequency dependence of Z'' at various temperatures of Zr doped Mn_3O_4 thin film deposited at various doping concentration.

of electric dipole in the direction of the applied field. Also, the enhancement of the σ_{dc} could be assigned to the presence of Mn^{3+} vacancies at octahedral sites leading to the creation of Mn^{4+} ions at the octahedral sites as reported previously by Bose and Biju (2015a) or else by the increase in drift mobility of charge carriers at higher temperatures as explained by Jain et al. (2016). Thus, according to our results, the gradual decrease in the activation energy with increase in conductivity confirms that the conduction is temperature dependent.

Power exponent "s". The evolution of the exponent of power "s" as a function of temperature is shown in Fig. 11 indicating the presence of three zones:

- A low temperatures; where the power exponent "s" is a constant and has value slightly greater than 1 indicating a super-linear character of the electrical conductivity. The invariance of "s" in this zone can be explained by the fact that the conduction is done by tunneling (quantum mechanical tunneling, QMT). In this model, "s" value is given by:

$$S = 1 - \frac{4}{Ln\left(\frac{1}{\omega\tau_0}\right)} \quad (10)$$

where τ_0 is the relaxation time of the jump between two sites, the product $\omega\tau_0$ is generally much greater than 1. Such a statement does not explain the fact that "s" is greater than 1. To explain this, it is necessary to take into consideration the thermal effect. In such situation, the form of "s" becomes:

$$S = 1 + \frac{4}{\frac{W}{kT} - Ln\left(\frac{1}{\omega\tau_0}\right)} \quad (11)$$

where W is the barrier height between two sites, a super-linear case is observed for:

$$\frac{W}{kT} > Ln\left(\frac{1}{\omega\tau_0}\right) \quad (12)$$

- An intermediate temperature zone; where the power exponent is slightly less than 1 and decreases with

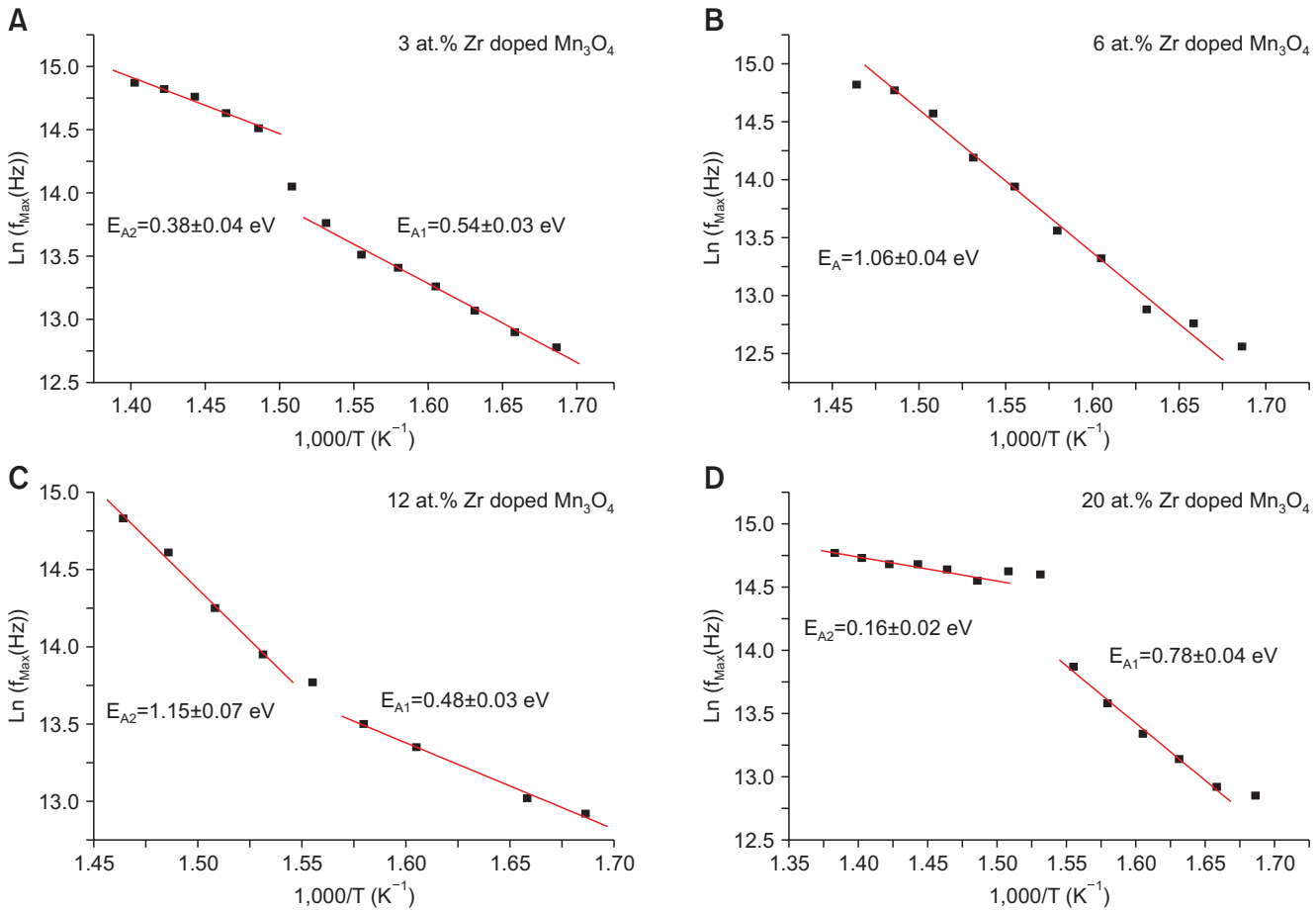

Fig. 17. Plot of $Ln(f_{Max})$ versus 1,000/T of Zr doped Mn_3O_4 films at various atomic concentration of Zr.

temperature. Such behavior is in good agreement with the CBH model. According to this model, "s" value can be written as:

$$S = 1 - \frac{6kT}{W_M - kTLn\left(\frac{1}{\omega\tau_0}\right)} \quad (13)$$

where W_M is the difference between the bipolaron level and the conduction band energy.

The variations of $\frac{1}{1-s}$ as a function of the inverse of the temperature (Fig. 13), allow us to obtain W_M value, which is about 1.5±0.2 eV, Table 3.

It is noted that the change of "s" behavior with the temperature is accompanied by a change of Z'' as a function of the frequency (f_{Max} passes from 2 kHz to 40 kHz). This behavior could be linked to the fact that an oxidation in air of Mn_3O_4 may occur to form Mn_2O_3 phase for temperatures of electrical measurements situated in 350°C~370°C domain. In fact, for this temperature interval the oxygen/manganese ratio varies in a moderate way (the value of O/Mn ratio increases from 1.33 to 1.50).

Indeed, we consider then the possibility of oxidation of Mn_3O_4 hausmanite thin film and its transformation into Mn_2O_3 and this is understood as a decrease of Mn^{2+} ions within Mn_3O_4 matrix according to the following reaction scheme:

$$2\ Mn_3O_4 + 1/2\ O_2 \rightarrow 3\ Mn_2O_3. \quad (14)$$

It is worth noting that this phase transformation due to oxidation is well-anticipated because, according to previous studies concerning manganese oxide materials, such a change is predictable by means of results conducted by Grundy et al. (2003) and Jacob et al. (2011). In the same line, this oxidation seems to be reinforced by the presence of Zr doping. Indeed, the disappearance of the plateau at T<350°C in the presence of Zr (as ZrO_x, ZrO_2 secondary phase inside the doped films) increases the oxidation process and hence the absence of the plateau for 12%~20% Zr content domain as mentioned in the following sections. Consequently, in undoped sample, the QMT model corresponds to Mn_3O_4 thin film while the CBH model is that of the transformed Mn_2O_3 layer in this latter where the conduction mechanism is provided by the large

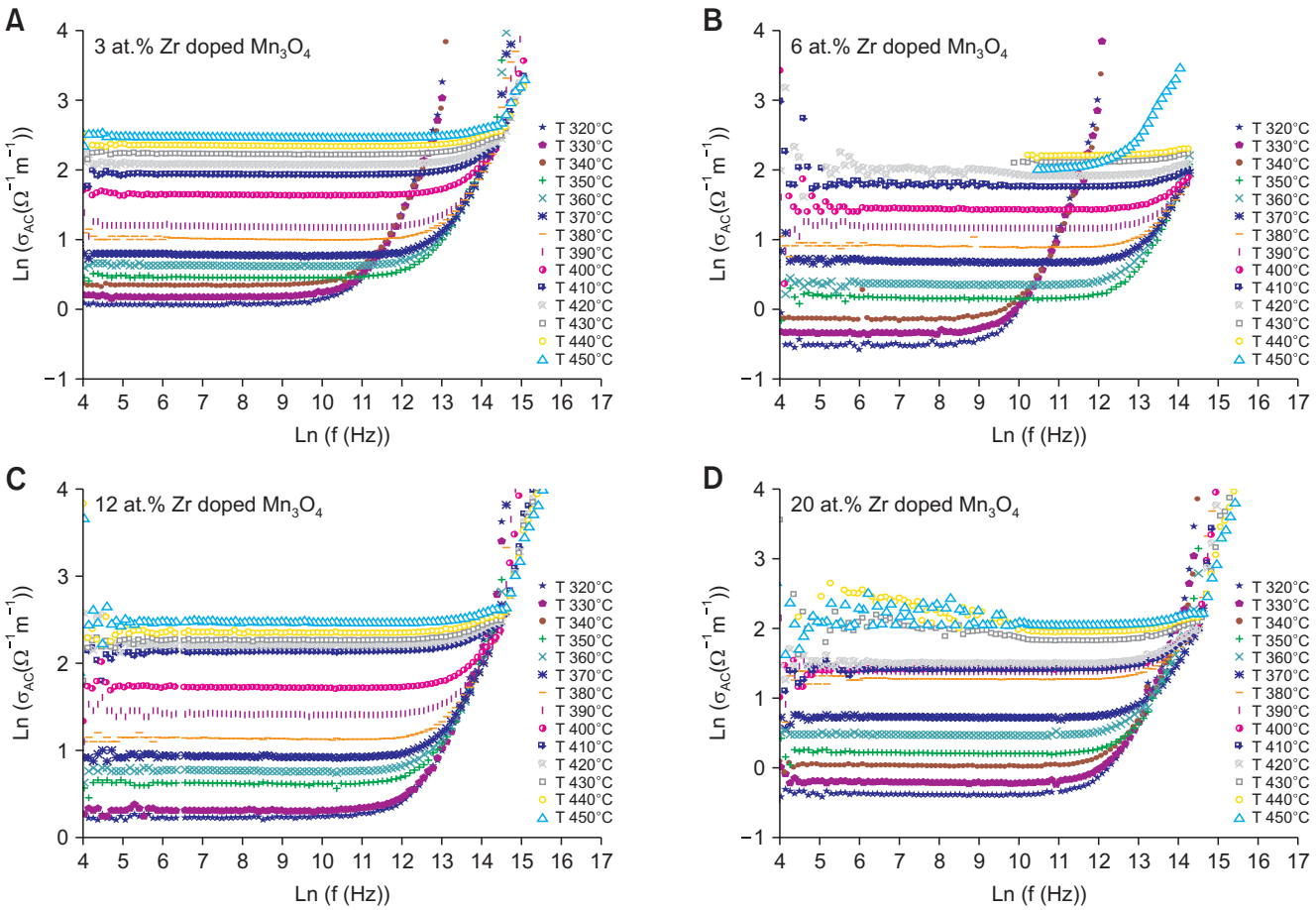

Fig. 18. Plot of ac conductivity as a function of frequency at different temperatures for Zr doped Mn_3O_4 at different temperatures.

polaron hopping, Fig. 14. For temperatures exceeding 400°C, the power exponent "s" has low values; this behavior can be explained in two different ways:

- at high temperatures domain, the density of free charges increases and consequently their contribution to conduction becomes preponderant (Conduction by the free charges is independent of the frequency), hence a decrease in the conduction dependence with frequency. Or/
- the conduction process as being is due to diffusion of thermally activated holes trapped at Mn^{3+} (following the formation of Mn_2O_3) rather than the charge carriers production. This assumption leads to the conclusion that the electrical conduction is due to an increase in the mobility of the charge carriers.

The effect of Zr doping in Mn_3O_4 thin films

The impedance analysis

The Nyquist diagrams of the different films of x at.% Zr doped Mn_3O_4 (with x=3, 6, 12, and 20) are represented in Fig. 15. It is found that as doping increases until 12 at.%, the diameter of the semicircle type arc which gives the electrical resistivity of the samples becomes more and more flattened proving that the distribution of relaxation time becomes increasingly wider leading to a decrease in resistivity. This decrease in resistivity which is probably due to an increase in the charge carriers concentration, could be attributed to the substitution of Mn^{2+} ions by Zr^{4+} ions as reported elsewhere (Funke, 1993) Such interpretation could be supported by previously reported theoretical studies that suggest that the formation energy of Zr_{Zn} defect is the lowest compared with that of interstitial Zr (Zr_i) and substitutional Zr for O (Zr_O). This indicates that Zr_{Zn} defect forms easier and its concentration may be the highest in doped films (Wang et al., 2008). However, when the doping reaches 20 at.%, the resistance increases again which could be explained by the fact that Zr element cannot incorporate into Mn_3O_4 matrix and it remains as an impurity in various forms of ZrO_x or ZrO_2, which lead (Herodotou et al., 2015; Lv et al., 2008; Paul et al., 2003; Wang et al., 2014). These results are consistent with those found elsewhere (Said et al., 2017). The curves giving

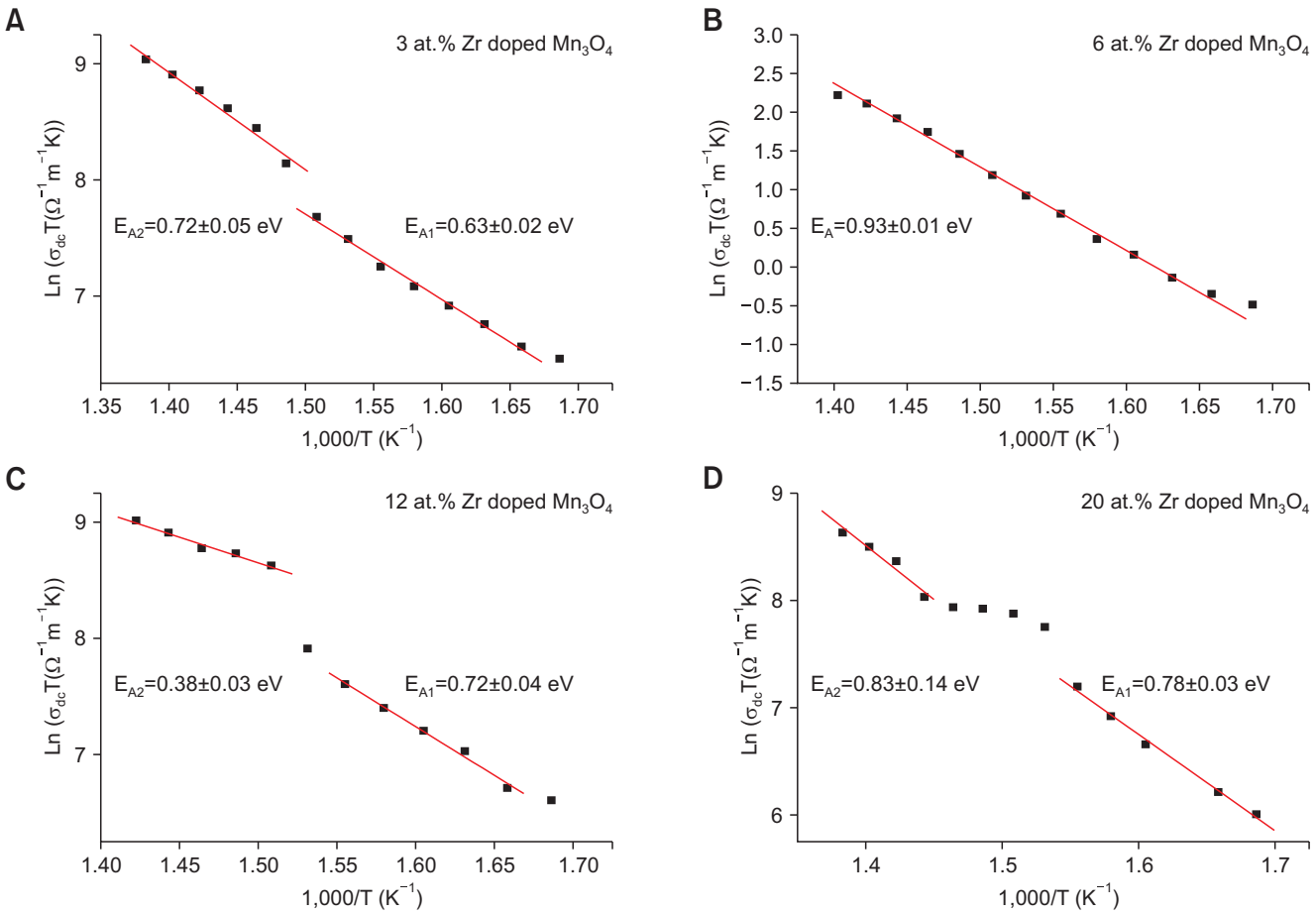

Fig. 19. Ln(T) versus 1,000/T for Zr doped Mn_3O_4.

the imaginary parts of the impedance as a function of the frequency for Zr doped Mn_3O_4 thin films (with x=3, 6, 12, 20) are also illustrated in Fig. 16. The relaxation frequencies fMax giving the maximum of Z'' increase with the temperature for all the samples following the Arrhenius law. It is also noted that in comparison with undoped Mn_3O_4, the amplitude of Z" decreases especially for 3 and 12 at.% Zr doped Mn_3O_4 samples, indicating possible accumulation of free charges in the grains further to the ionization of the Zr atoms on Mn-sites, where Zr^{4+} ions replace Mn^{2+} ions giving two extra electrons to the system. Always in comparison with undoped Mn_3O_4 thin film, doped ones have the relaxation frequency f_{Max} shifting to higher frequencies showing a noticeably decrease in phonon's relaxation time. As a matter of fact, the dielectric relaxation time is closely related to the electrical conductivity. Indeed, it is a measure of how long relaxation phenomenon takes to become neutralized by conduction process. This being so, one could conclude that zirconium doping could reinforce the metallic character of these films. On the other hand, the curves related to $Ln(f_{Max})$ as a function of 1/T for different films are displayed in Fig. 17. The corresponding activating energies are indicated on the curves and gathered. It is noted that, with the exception of 6 at.% Zr doped Mn_3O_4, the different films possess 2 activating energies: the first is related to low temperatures domain and the second is for high temperatures one. These energies do not exhibit a constant monotone with the Zr content which may be due to three plausible reasons:

- possible incorporation of Zr into Mn_3O_4,
- possible moving of Zr ions from their interstitial sites to form ZrO_x entities as secondary phases or/
- Zr might reached solubility limit in Mn_3O_4 matrix. In fact, at low temperatures, the increased of oxygen induced by Zr_{Mn} and Zr_i are short range motion at relatively low Zr content (except for 6 at.%).

As a result, E_{A1} gives minimum value in this doping range. However, at the highest doping level (i.e., 20 at.%), the oxygen is pinned by Zr that moved from their interstitial sites to clusters and form secondary phases and became long range motion, reducing thus the diffuseness of Zr. Consequently, E_{A1} reached a high value of about 0.87 eV which corresponds to the activation energy of conduction caused by oxygen

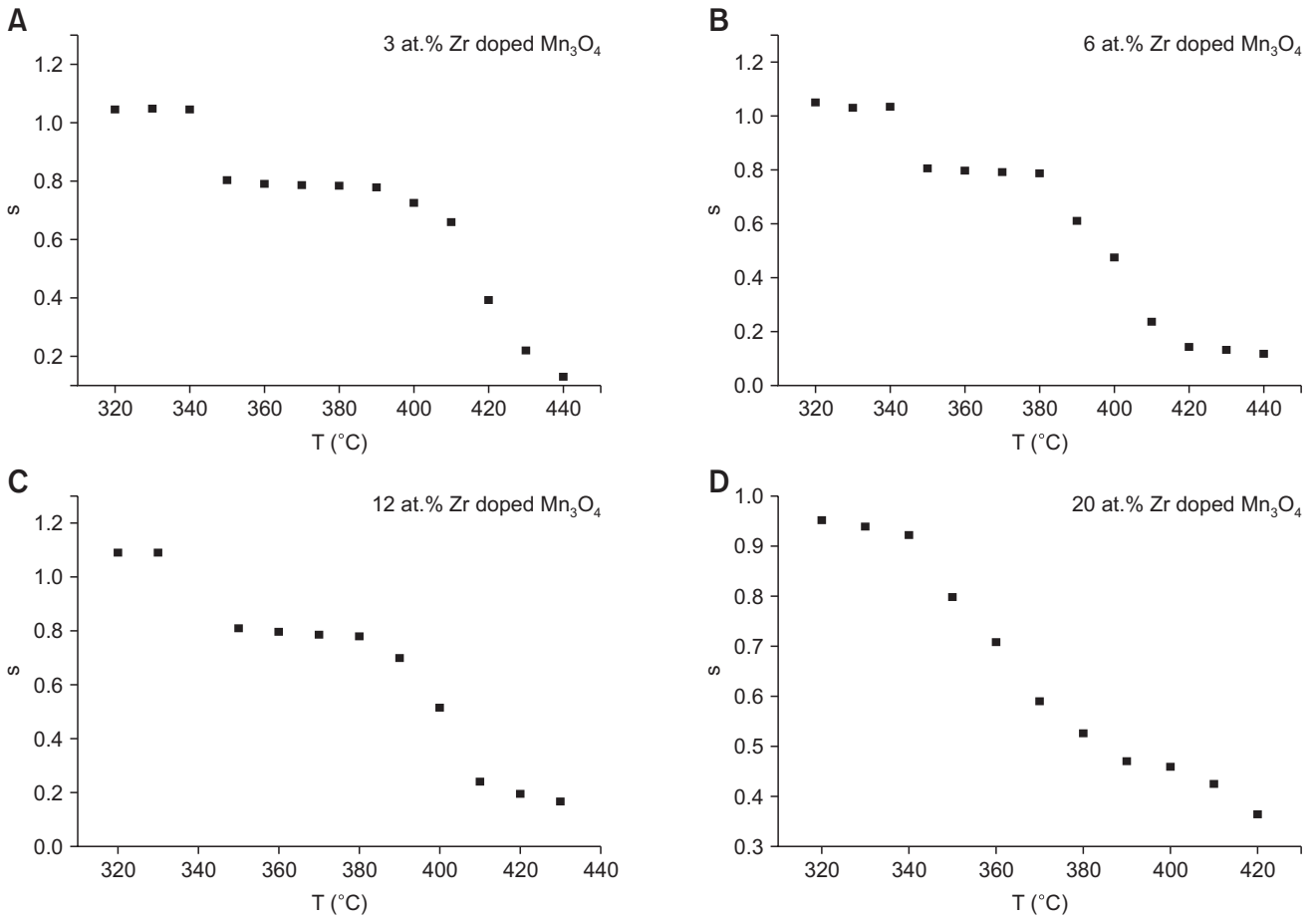

Fig. 20. Temperature dependence of the 's' parameter for different doping level.

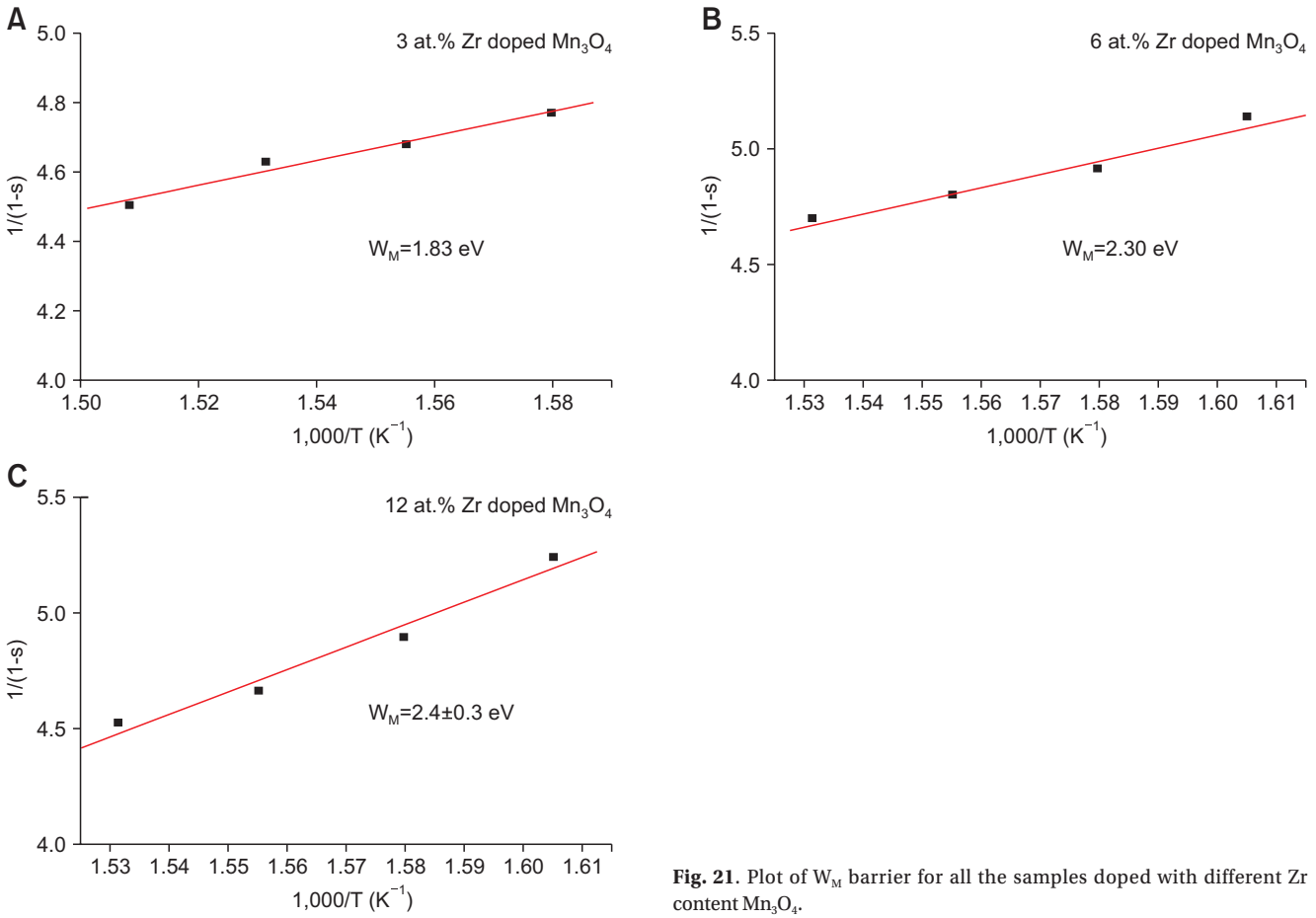

Fig. 21. Plot of W_M barrier for all the samples doped with different Zr content Mn_3O_4.

vacancies, that is around 1 eV. Moreover, the increase of the temperature has an intricate influence on E_{A2} activation energy. In fact, the ionic diffusion via the structural defaults and interstitial atoms in addition to impurities depend strongly on the temperature. In view of these intricacies, we do not have a reliable explication of high temperature influence on the activation energy because the phenomena overlap and we cannot isolate each of them.

Conductivity study

ac conductivity. The curves displayed in Fig. 18 give the variations of the conductivity in terms of the frequency for different Zr doped Mn_3O_4 thin films. It is found that in low temperatures (<350°C) for which the activation is carried out at low frequency (~2 kHz), it remains for the doped films having concentrations of 3 and 6 at.% and disappears for Zr 20% doped film. This can be explained by the fact that Zr doping blocks the oxidation of Mn_3O_4 to form Mn_2O_3 and thus opposes the insertion of the oxygen into the layer as as it is detailed above (see Power exponent "s" subsection, 140 pages).

σ_{dc} behavior. The variations of the conductivity measurements, at low frequencies, as a function of the inverse of the temperature are represented in the Fig. 19. We note that, as for $Ln(f_{Max})$, with the exception of 6 at.% Zr-doped Mn_3O_4, the measurements show two energies of activations corresponding to low and high temperatures. These energies present indeed an absence of monotony feature with Zr concentration. The activation energies, whether at low or high temperatures are close and quite high values compared to those found by the frequency study which could be explained by a long range nature of relaxation process.

Power exponent "s". The variations of the power exponent "s" as a function of the temperature for different Zr doping are shown in Fig. 20.

We notice indeed the following relevant facts:

- The super-linear conduction zone has disappeared for 20 at.% Zr doped film which reinforces the idea that the oxidation of Mn_3O_4 to Mn_2O_3 has been blocked by the use of a relatively high Zr content.
- In the intermediate zone (350°C~390°C) especially for the 3, 6, and 12 at.% Zr doped films, the conduction admits

always a mechanism according to CBH model with a greater barrier W_M (Fig. 21), indicating that the defaults level approximates the valence band one.

CONCLUSIONS

In summary, we have addressed the issues regarding the change of the electric mechanisms within Zr doped Mn_3O_4 hausmanite thin films through an oxidation in air around the temperature of the order of 350°C. This contribution seems so interesting to illuminate some intrigue phenomena concerning the stability of such binary oxide material with respect to an oxidation caused by the annealing temperature. Such electrical investigations which have so far been thoroughly addressed in this work may be of interest for possible use of these films in several interesting applications which have recently emerged at the forefront of potentials research such as the photocatalysis, gas and bio-sensors and so on.

CONFLICT OF INTEREST

No potential conflict of interest relevant to this article was reported.

REFERENCES

Aghayan M, Zak A K, Behdani M, and Hashim A M (2014) Sol–gel combustion synthesis of Zr-doped $BaTiO_3$ nanopowders and ceramics: Dielectric and ferroelectric studies. *Ceramics International* **40**, 16141-16146.

Alonso-Domínguez D, Álvarez-Serrano I, López M L, Cuello Gabrie I J, Asensio E, García-Hernández M, Veiga M L, and Pico C (2016) Characterization of $SrBiMn_{2-x}Ti_xO_6$ perovskites: Local ordering influence on the dielectric and magnetic response. *Ceramics International* **42**, 11889-11900.

Baghizadeh A, Vieira J M, Amaral J S, Graça M P, Soares M R, Mota D A, and Amaral V S (2015) Crystal structure, magnetic and dielectric behavior of h-$LuMn_xO_{3\pm\delta}$ ceramics ($0.95 \leq x \leq 1.04$). *Journal of Magnetism and Magnetic Materials* **395**, 303-311.

Bai W, Chen D, Zhang J, Zhong J, Ding M, Shen B, Zhai J, and Ji Z (2016) Phase transition behavior and enhanced electromechanical properties in $(Ba_{0.85}Ca_{0.15})(Zr_xTi_{1-x})O_3$ lead-free piezoceramics. *Ceramics International* **42**, 3598-3608.

Belgacem S and Bennaceur R (1990) Propriétés optiques des couches minces de SnO_2 et $CuInS_2$ airless spray. *Rev. Phys. Appl.* **25**, 1245.

Biju V and Khadar M A (2003) Dielectric properties of nanostructured nickel oxide. *Journal of Materials Science* **38**, 4055-4063.

Bose V C and Biju V (2015a) Optical, electrical and magnetic properties ofnanostructured Mn_3O_4 synthesized through a facile chemical route. *Physica E* **66**, 24-32.

Bose V C and Biju V (2015b) Defect dependent optical, electrical and magnetic properties of nanostructured Mn_3O_4. *Superlattices and Microstructures* **88**, 287-298.

Boukhachem A, Ziouche A, Amor M B, Kamoun O, Zergoug M, Maghraoui-Meherzi H, Yumak A, Boubaker K, and Amlouk M (2016) Physical investigations on perovskite LaMnO3-d sprayed thin films for spintronic applications. *Materials Research Bulletin* **74**, 202-211.

Caglara Y, Ilican S, and Caglar M (2007) Single-oscillator model and determination of optical constants of spray pyrolyzed amorphous SnO_2 thin films. *Eur. Phys. J. B* **58**, 251-256.

Chang Y Q, Yu D P, Long Y, Xu J, Luo X H, and Ye R C (2005) Large-scale fabrication of single-crystalline Mn_3O_4 nanowires via vapor phase growth. *J. Crystal Growth* **279**, 88-92.

DiDomenico M, Eibschütz M, Guggenheim H J, and Camlibel I (1969) Dielectric behavior of ferroelectric $BaMF_4$ above room temperature. *Solid State Comm.* **7**, 1119-1122.

Dong R, Ye Q, Kuang L, Lu X, Zhang Y, Zhang X, Tan G, Wen Y, and Wang F (2013) Enhanced supercapacitor performance of Mn_3O_4 nanocrystals by doping transition-metal ions. *ACS Appl. Mater. Inter.* **5**, 9508-9516.

Dridi R, Saafi I, Mhamdi A, Matri A, Yumak A, Haj Lakhdar M, Amlouk A, Boubaker K, and Amlouk M (2015) Structural, optical and AC conductivity studies on alloy $ZnO–Zn_2SnO_4$ (ZnO–ZTO) thin films. *Journal of Alloys and Compounds* **634**, 179-186.

Funke K (1993) Jump relaxation in solid electrolytes. *Prog. Solid State Chem.* **22**, 111.

Gogoi P, Kumar T S, Sharma P, and Pamu D (2015) Structural, optical, dielectric and electrical studies on RF sputtered nanocrystalline Zr doped $MgTiO_3$ thin films. *Journal of Alloys and Compounds* **619**, 527-537.

Grundy A N, Hallstedt B, and Gauckler L J (2003) Assessment of the Mn-O system. *Journal of Phase Equilibria* **24**, 21-39.

Gund G S, Dubal D P, Patil B H, Shinde S S, and Lokhande C D (2013) Enhanced activity of chemically synthesized hybrid graphene oxide/Mn_3O_4 composite for high performance supercapacitors. *Electrochim. Acta* **92**, 205-215.

Herodotou S, Treharne R E, Durose K, Tatlock G J, and Potter R J (2015) The effects of Zr doping on the optical, electrical and microstructural properties of thin ZnO films deposited by atomic layer deposition. *Materials* **8**, 7230-7240.

Hou Q, Zhao C, and Xu Z (2016) Effect of Zr doping on the electrical and optical properties of ZnO. *Chemical Physics Letters* **658**, 336-342.

Huang S, Wang Y, Wang Z, Zhao K, Shi X, Lai X, and Zhang L (2015) Structural, magnetic and magnetodielectric properties of the Mn_3O_4 thin films epitaxially grown on $SrTiO_3$ (001) substrates. *Solid State Comm.* **212**, 25-29.

Jacob K T, Kumar A, Rajitha G, and Waseda Y (2011) Thermodynamic data for Mn_3O_4, Mn_2O_3 and MnO_2. *High Temp. Mater. Proc.* **30**, 459-472.

Jain A, Saroha R, Pastor M, Jha A K, and Panwar A K (2016) Effect of sintering duration on structural and electrical properties of $Ba_{0.9}Sr_{0.1}Ti_{0.96}Zr_{0.04}O_3$ solid solution. *Current Applied Physics* **16**, 859-

866.

Jha A, Thapa R, and Chattopadhyay K K (2012) Structural transformation from Mn_3O_4 nanorods to nanoparticles and band gap tuning via Zn doping. *Mater. Res. Bull.* **47**, 813.

Jin G, Xiao X, Li S, Zhao K, Wu Y, Sun D, and Wang F (2015) Strongly coupled graphene/Mn_3O_4 composite with enhanced electrochemical performance for supercapacitor electrode. *Electrochim. Acta* **178**, 689-698.

Juma A, Acik I O, Oluwabi A T, Mere A, Mikli V, Danilson M, and Krunks M (2016) Zirconium doped TiO_2 thin films deposited by chemical spray pyrolysis. *Applied Surface Science* **387**, 539-545.

Khumpaitool B and Khemprasit J (2014). Effect of calcining temperature on structural and dielectric properties of $Li_{0.30}Cr_{0.02}Ni_{0.68}O$ ceramics. *Journal of Alloys and Compounds* **587**, 211–216.

Larbi T, Amara A, Said L B, Ouni B, Lakhdar M H, and Amlouk M (2015a) A study of optothermal and AC impedance properties of Cr-doped Mn_3O_4 sprayed thin film. *Materials Research Bulletin* **70**, 254-262.

Larbi T, Lakhdar M H, Amara A, Ouni B, Boukhachem A, Mater A, and Amlouk M (2015b) Nickel content effect on the microstructural, optical and electrical properties of p-type Mn_3O_4 sprayed thin films. *Journal of Alloys and Compounds* **626**, 93-101.

Larbi T, Ouni B, Boukhachem A, Boubaker K, and Amlouk M (2014) Investigation of structural, optical, electrical and dielectric properties of catalytic sprayed hausmannite thin film. *Materials Research Bulletin* **60**, 457-466.

Lee K J, Iguchi A, and Iguchi E (1993) Polaronic conduction of electrons in α-Mn_3O_4 slightly doped with Li. *J. Phys. Chem. Solids* **54**, 975.

Lin K C, Juan P C, Liu C H, Wang M C, and Chou C H (2015) Leakage current mechanism and effect of Y_2O_3 doped with Zr high-K gate dielectrics. *Microelectronics Reliability* **55**, 2198-2202.

Liu J Y, Ng Y H, Okatan M B, Amal R, Bogle K A, and Valanoor N (2014) Interface-dependent Electrochemical Behavior of Nanostructured Manganese (IV) Oxide (Mn_3O_4). *Electrochim. Acta* **130**, 810-817.

Luo Y, Yang T, Li Z, Xiao B, and Zhang M (2016) High performance of Mn_3O_4 cubes for supercapacitor applications. *Materials Letters* **178**, 171-174.

Lv M, Xiu X, Pang Z, Dai Y, Ye L, Cheng, C, and Han S (2008) Structural, electrical and optical properties of zirconium-doped zinc oxide films prepared by radio frequency magnetron sputtering. *Thin Solid Film.* **516**, 2017-2021.

Mahajan S, Haridas D, Ali S T, Munirathnam N R, Sreenivas K, Thakur O P, and Prakash C (2014) Investigation of conduction and relaxation phenomena in $BaZr_xTi_{1-x}O_3$ (x=0.05) by impedance spectroscopy. *Physica B* **451**, 114-119.

Manoharan C, Jothibas M, Jeyakumar S J, and Dhanapandian S (2015) Structural, optical and electrical properties of Zr-doped In_2O_3thin films. *Spectrochimica Acta Part A: Molecular and Biomolecular Spectroscopy* **145**, 47-53.

Mardare D and Hones P (1999) Optical dispersion analysis of TiO_2 thin films based on variable-angle spectroscopic ellipsometry measurements. *Mater. Sci. Eng. B,* **68**, 42.

Mohamed J J, Salim S A S, and Ahmad Z A (2016) Comparative study on the effect of Zr^{4+} and Ca^{2+} doping on the properties of NiO. *Procedia Chemistry* **19**, 949-954.

Mrabet C, Amor M B, Boukhachem A, Amlouk M, and Manoubi T (2016) Physical properties of La-doped NiO sprayed thin films for optoelectronic and sensor applications. *Ceramics International* **42**, 5963-5978.

Mrabet C, Kamoun O, Boukhachem A, Amlouk M, and Manoubi T (2015) Some physical investigations on hexagonal-shaped nanorods of lanthanum-doped Zn. *Journal of Alloys and Compounds* **648**, 826-837.

Myung J, Shin TH, Huang X, Carins G, and Irvine J T S (2015) Enhancement of redox stability and electrical conductivity by doping various metals on ceria, $Ce_{1-x}MxO_{2-\delta}$ (M = Ni, Cu, Co, Mn, Ti, Zr). *International Journal of Hydrogen Energy* **40**, 12003-12008.

Nicon C, Soares M R N, Costa L C, Monteiro T, and Graça M P F (2016) Effects of Zr and Ga doping on the stoichiometry and properties of niobium oxides. *Ceramics International* **42**, 1688-1697.

Ouni B, Boukhachem A, Dabbous S, Amlouk A, Boubaker K, and Amlouk M (2010) Some transparent semi-conductor metal oxides: Comparative investigations in terms of Wemple–DiDomenico parameters, mechanical performance and Amlouk–Boubaker optothermal expansivity. *Materials Science in Semiconductor Processing* **13**, 281-287.

Pang L-X, Zhou D, Liu W-G, and Yue Z-X (2016) Phase evolution and dielectric properties of fluorite-type $Bi_3(Nb_{0.9}M_{0.1})O_{7+\delta}$ ceramics (M=Ti, Zr, Sn, W, δ=±0.05). *Journal of Alloys and Compounds* **674**, 89-92.

Park W-D (2012) Optical constants and dispersion parameters of CdS thin film prepared by chemical bath deposition. *Transactions on Electrical and Electronic Materials* **13**, 196-199.

Paul G K, Bandyopadhyay S, Sen S K, and Sen S (2003) Structural, optical and electrical studies on sol–gel deposited Zr doped ZnO films. *Mater. Chem. Phys.* **79**, 71-75.

Rouahi A, Challali F, Dakhlaoui I, Vallée C, Salimy S, Jomni F, Yangui B, Besland M P, Goullet A, and Sylvestre A (2016) Structural and dielectric characterization of sputtered Tantalum Titanium Oxide thin films for high temperature capacitor applications. *Thin Solid Films* **606**, 127-132.

Said L B, Inoubli A, Bouricha B, and Amlouk M (2017) High Zr doping effects on the microstructural and optical properties of Mn_3O_4 thin films along with ethanol sensing. *Spectrochimica Acta Part A: Molecular and Biomolecular Spectroscopy* **171**, 487-498.

Saini J, Kumar R, Rajput J K, and Kumar A (2016) Study of $Zr_xZn_{0.5-x}Ni_{0.5}Fe_2O_4$ $0 \leq x \leq 0.25$: synthesis, structural, magnetic and electrical properties. *Journal of Magnetism and Magnetic Materials* **401**, 770-774.

Salah M, Azizi S, Boukhachem A, Khaldi C, Amlouk M, and Lamloumi J (2017) Structural, morphological, optical and photodetector properties of sprayed Li-doped ZnO thin films. *Journal of Materials Science* **52**, 10439-10454.

Saputra E, Muhammad S, Sun H, Ang H-M, Tade M O, and Wang S (2013) A comparative study of spinel structured Mn_3O_4, Co_3O_4 and Fe_3O_4 nanoparticles in catalytic oxidation of phenolic contaminants in aqueous solutions. *Journal of Colloid and Interface Science* **407**, 467-473.

Shanmugam V, Sridarane R, Deviannapoorani C, Kashyap R, and Murugan R (2014) Influence of zirconium doping on structure, microstructure, dielectric and impedance properties of strontium bismuth niobate ceramics. *Current Applied Physics* **14**, 407-414.

Sharma J K, Srivastava P, Ameen S, Akhtar M S, Singh G, and Yadava S (2016) *Azadirachta indica* plant-assisted green synthesis of Mn_3O_4 nanoparticles: Excellent thermal catalytic performance and chemical sensing behavior. *Journal of Colloid and Interface Science* **472**, 220-228.

Slassi A, Iakouari N, Ziat Y, Zarhri Z, Fakhim Lamrani A, Hlil E K, and Benyoussef A (2015) Ab initio study on the electronic, optical and electrical properties of Ti-, Sn- and Zr-doped ZnO. *Solid State Communications* **218**, 45-48.

Sun L, Wang Z, Hao W, Cao E, Zhang Y, and Peng H (2015) Influence of Zirconium doping on microstructure and dielectric properties of $CaCu_3Ti_4O_{12}$ synthesized by the sol–gel method. *Journal of Alloys and Compounds* **651**, 283-289.

Sun Z, Pu Y, Dong Z, Hu Y, Liu X, and Wang P (2014) Effect of Zr^{4+} content on the T_c range and dielectric and ferroelectric properties of $BaZr_xTi_{1-x}O_3$ ceramics prepared by microwave sintering. *Ceramics International* **40**, 3589-3594.

Tang X G, Chew K H, and Chan H L W (2004) Diffuse phase transition and dielectric tunability of $Ba(Zr_yTi_{1-y})O_3$ relaxor ferroelectric ceramics. *Acta Mater.* **52**, 5177-5183.

Thongbai P, Jumpatam J, Putasaeng B, Yamwong T, and Maensiri S (2014) Microstructural evolution and Maxwell–Wagner relaxation in $Ca_2Cu_2Ti_{4-x}Zr_xO_{12}$: The important clue to achieve the origin of the giant dielectric behavior. *Materials Research Bulletin* **60**, 695-703.

Ulutas C, Erken O, Gunes M, and Gumus C (2016) Effect of annealing temperature on the physical properties of Mn_3O_4 thin film prepared by chemical bath deposition. *Int. J. Electrochem. Sci.* **11**, 2835-2845.

Wang F, Lv M, Pang Z, Yang T, Dai Y, and Han S (2008) Theoretical study of structural, optical and electrical properties of zirconium-doped zinc oxide. *Applied Surface Science* **254**, 6983-6986.

Wang F, Wu H Q, Lin Z T, Han S Y, Wang D, Xue Y, Sun Y L, Sun J, and Li B (2010) Shape evolution of Cu-doped Mn_3O_4 spinel microcrystals: influence of copper content. *Mater. Res. Bull.* **45**, 1567.

Wang Z, Wang Z, Peng W, Guo H, and Li X (2014) An improved solid-state reaction to synthesize Zr-doped $Li_4Ti_5O_{12}$ anode material and its application in $LiMn_2O_4/Li_4Ti_5O_{12}$ full-cell. *Ceramics International* **40**, 10053-10059.

Wei T, Wang X D, Zhao C Z, Zhang T B, Yang F M, Wang W B, and Ma Y J (2015) Enhanced up-conversion photoluminescence and dielectric properties of Er- and Zr-codoped strontium bismuth niobate ceramics. *Ceramics International* **41**, 12364-12370.

Wei W, Cui X, Chen W, and Ivey D G (2011) Manganese oxide-based materials as electrochemical supercapacitor electrodes. *Chem. Soc. Rev.* **40**, 1697.

Wemple S H and DiDomenico M (1971) Behavior of the electronic dielectric constant in covalent and ionic materials. *Phys. Rev. B,* **3**, 1338.

Wypych A, Bobowska I, Tracz M, Opasinska A, Kadlubowski S, Krzywania-Kaliszewska A, Grobelny J, and Wojciechowski P (2014) Dielectric properties and characterisation of titanium dioxide obtained by different chemistry methods. *Journal of Nanomaterials* **124814**, 9.

Xu G, Shi J, Dong W, Wen Y, Min X, and Tang A (2015) One-pot synthesis of a Ni–Mn_3O_4 nanocomposite for supercapacitors. *Journal of Alloys and Compounds* **630**, 266-271.

Xu H Y, Le Xu S, Li X D, Wang H, and Yan H (2006) Chemical bath deposition of hausmannite Mn_3O_4 thin films. *Appl. Surf. Sci.* **252**, 4091-4096.

Yadav A A, Jadhav S N, Chougule D M, Patil P D, Chavan U J, and Kolekar Y D (2016) Spray deposited Hausmannite Mn_3O_4 thin films using aqueous/organic solvent mixture for supercapacitor applications. *Electrochimica Acta* **206**, 134-142.

Yang X, He Y, Bai Y, Zhang J, Kang L, Xu H, Shi F, Lei Z, and Liu Z-H (2016) Mn_3O_4 nanocrystalline/graphene hybrid electrode with high capacitance. *Electrochimica Acta* **188**, 398-405.

Zhang B, Dong X, Xu X, Zhao P, and Wu J (2008) Characteristics of zirconium-doped indium tin oxide thin films deposited by magnetron sputtering. *Solar Energy Materials & Solar Cells* **92**, 1224-1229.

Zhao Y, Ran W, Xiong D-B, Zhang L, Xu J, and Gao F (2014) Synthesis of Sn-doped Mn_3O_4/C nanocomposites as supercapacitor electrodes with remarkable capacity retention. *Mater. Lett.* **118**, 80-83.

Zhen M, Zhang Z, Ren Q, and Liu L (2016) Room-temperature synthesis of ultrathin Mn_3O_4 nanosheets as anode materials for lithium-ion batteries. *Materials Letters* **177**, 21-24.

Zhi Y, Guo R, and Bhalla A S (2000) Dielectric behavior of $Ba(Ti_{1-x}Zr_x)O_3$ Ba $(Ti_{1-x}Zr_x)$ O_3 single crystals. *J. Appl. Phys.* **88**, 410.